Large-Scale Molecular Dynamics Simulations of Three-Dimensional Ductile Failure

S. J. Zhou, D. M. Beazley, P. S. Lomdahl, and B. L. Holian
Theoretical Division and Center for Nonlinear Studies, Los Alamos National Laboratory, Los Alamos, New Mexico 87545
(Received 28 June 1996)

We have performed massively parallel 3D molecular dynamics simulations with up to 35 million atoms to investigate ductile failure, obtaining mechanistic information at the atomistic level inaccessible to experiment. We observe dislocation loops emitted from the crack front—the first time this has been seen in computer simulations. The sequence of dislocation emission events, essential for establishing an intrinsic ductility criterion, strongly depends on the crystallographic orientation of the crack front and differs strikingly from anything previously conjectured. [S0031-9007(96)01980-1]

PACS numbers: 61.72.Lk, 61.72.Yx, 62.20.Fe, 62.20.Mk

Understanding the failure mechanisms in materials is crucial to the development of new materials with high strength and toughness. Cracks and dislocations are the two major defects determining these mechanical properties. While continuum theory can successfully describe the long-range strain fields of cracks and dislocations, atomistic simulations are required to characterize their core regions. In the past, because only a small number of atoms could be simulated, various boundary treatments were employed to provide a static crack stress field (e.g., [1,2]). In addition to their lack of dynamic response, those boundary treatments are only valid until the first dislocation travels a small fraction of the computational cell away from the crack tip. Furthermore, intrinsic three-dimensional (3D) features of dislocations and cracks cannot be properly investigated with only a few atoms allocated in the direction along the crack front. With the advent of massively parallel computers, simulations of many millions of atoms in 3D are now feasible [3], allowing us to avoid using, at least for early times, complicated boundary treatments [4]. We have developed a 3D MD code, SPaSM (scalable parallel short range molecular dynamics), designed for very large-scale simulations on a variety of parallel computing platforms [3]. In addition to the computation of the many-body trajectory, SPaSM allows us to visualize, filter, and analyze the huge amount of data produced from a simulation of millions of atoms, perhaps the most challenging problem encountered in large-scale computer simulations.

To demonstrate the effectiveness of this new powerful tool and to investigate failure mechanisms, we have simulated the process of dislocation emission from a 3D crack. Crack blunting by dislocation emission enhances the ductility of crystalline materials [5]. There are two kinds of 3D dislocation emission processes: blunting and jogging. In the blunting configuration the dislocation is on a slip plane inclined to the crack plane and containing the crack front. The emission causes the crack to blunt in the direction of the Burgers vector **b**. In the jogging configuration, the slip plane is oblique to the crack front, and the emission makes a jog in the crack front in the direction of **b**. Blunting lowers the stress concentration at the crack front and hinders the propagation of the crack, thus making the material tough. Jogging results in a step or a dragging point for the crack. In addition to these geometrical changes, dislocation loops also shield or antishield cracks (i.e., reduce or increase the stress intensity factor at the crack tip). The driving force for emission of a blunting dislocation is large because a flat dislocation loop can release more strain energy by being as close to the crack front as possible [6]. On the other hand, there is probably less resistance to the emission of a jogging dislocation, since it does not create new surface like the blunting dislocation. While both jogging and blunting dislocations have been observed in experiments [7,8], the theoretical picture is much less clear [6,9–12]. In this paper, we present computer experimental results that shed light on the sequence of 3D dislocation emission events at crack tips.

In our MD simulations the atoms interact either via Morse pair potentials, differing in stiffness parameter, α, or via a more realistic embedded atom method (EAM) many-body potential, appropriate to copper [13]. Throughout, we use as units the atomic mass m, distance r_0 between nearest neighbors in the zero-temperature and zero-pressure crystal, and bond energy ε; hence the unit of time t_0 ($\sim$2.5 vibrational periods, or $\sim 10^{-12}$ sec) is given by $\varepsilon = m r_0^2/t_0^2$; the time step is $0.01 t_0$. In these units, the Morse pair potential is written as $\phi(r) = e^{-2\alpha(r-1)} - 2e^{-\alpha(r-1)}$ with a cutoff at $r_{\max} = 2.5 r_0$. In this paper, we will concentrate on exploring mechanical aspects of dislocation emission without thermal fluctuations, so we set the initial temperature to nearly zero ($10^{-6}\varepsilon/k$). The atoms are initially placed in perfect face-centered-cubic (fcc) crystal lattice sites. Dislocation emission from a crack is relatively easy in fcc crystals, and interatomic potentials for fcc metals are well characterized. The crystal orientation of our fcc system is shown in Fig. 1, including the (010) crack plane and {111} slip planes. In fcc metals of relatively low stacking fault energy, including copper, slip dislocations on the close-packed {111} planes are in extended configurations, consisting of two Shockley partial dislocations separated by a stacking fault ribbon (see Fig. 2).

In our MD simulations, we use a large computational cell with periodic boundary conditions in the x and y

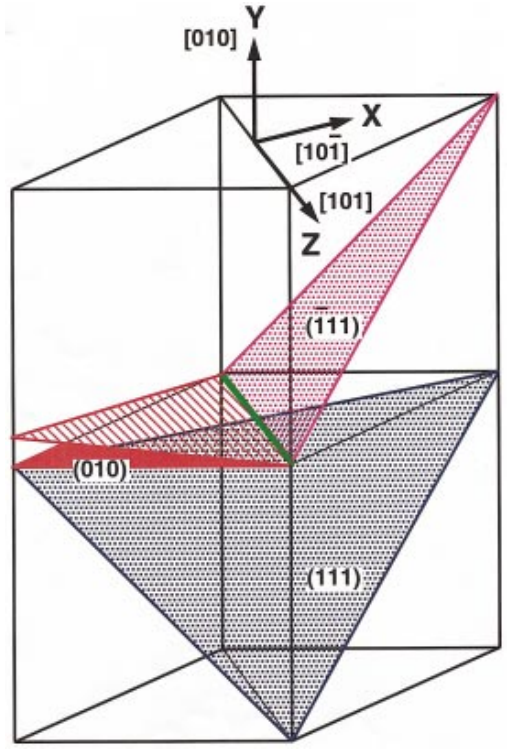

FIG. 1(color). The crack plane is on (010) and crack front is along [101]. One set of {111} slip planes, e.g., ($\bar{1}$11), contains the crack front and the others, e.g., (111), do not.

directions in order to preserve the long-range character of the crack and dislocation strain fields. We save computation time by initially embedding an atomistically sharp equilibrium crack (loaded at the Griffith critical strain ϵ_c), displacing atoms according to the continuum elastic solution for a finite crack in an unbounded solid. System sizes ranged from 1.7 to 35 million atoms, where the dimensions are $240 \times 425 \times 240$, with a crack length of 81, such that the shortest distance between periodic-image crack tips is 160, requiring a time of $\sim 30t_0$ for sound-wave communication.

Various numbers of planes were chosen in the z direction to explore 3D effects. The shortest half crack length of the sharp initial crack was $20r_0$, which is long enough to have the crack strain field be close to that of a continuum crack. We produce a crack that initially lies on the x-z plane under uniaxial remote loading strain ϵ_0 (just below ϵ_c) in the y direction (see Fig. 1). We gradually increase the loading strain by applying a homogeneous strain rate, where the x-z periodic boundary planes move apart from each other at constant velocity. **(**Adiabatic uniaxial expansion, at least at the rates accessible to MD simulations, produces conditions similar to those found in shockwave-induced spallation experiments [14].**)** The atoms first readjust their initial positions given by elastic theory, ending up with more rounded crack tips. The crack extends forward by no more than two lattice spacings, whereupon dislocation loops are eventually nucleated without further crack extension.

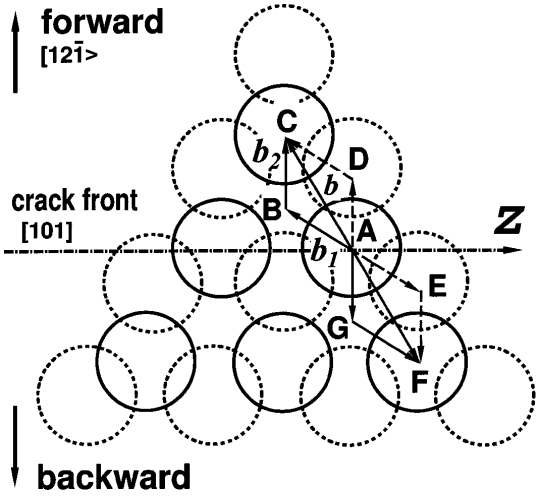

FIG. 2. Two atomic layers of a ($\bar{1}$11) slip plane show the permitted pathways of the forward ($A \rightarrow B \rightarrow C$) and backward ($A \rightarrow G \rightarrow F$) motions, relative to the crack propagation direction, for the perfect dislocation. Motion from A to D or from A to E is energetically forbidden by the existence of atoms D and E. The perfect dislocation with Burgers vector $b = 1/2[01\bar{1}]$ and its two partial dislocations with Burgers vectors $b_1 = 1/6[\bar{1}1\bar{2}]$ and $b_2 = 1/6[12\bar{1}]$ are shown. For a unit length of dislocation, the driving force is $\mathbf{F} = (\mathbf{b} \cdot \boldsymbol{\sigma}) \times \boldsymbol{\xi}$, where $\boldsymbol{\sigma}$ is the stress tensor, and $\boldsymbol{\xi}$ is the unit vector describing the dislocation line direction. For blunting dislocation emission, $F = b_r \sigma_{r\theta}$, where b_r is the radial component in the x-y plane of $\mathbf{b}$ and $\sigma_{r\theta} \propto \sin(\theta/2)\cos^2(\theta/2)$. The angles θ between the inclined ($\bar{1}$11) slip plane and the crack plane are 54.73° and 125.27° for forward and backward partial dislocation emission, respectively. Therefore the ratio of F_{backward} to F_{forward} is 1.034.

For a 3D crack at equilibrium, the vicinity of a free boundary surface normal to the z axis is under plane stress: the stress $\sigma_{zz} = 0$ and the strain $\epsilon_{zz} \neq 0$; while the bulk is under plane strain: the displacement $u_z = 0$. According to linear elastic fracture mechanics, the maximum shear stress under plane stress is on planes through the x axis subtending an angle of 45° with the x-z plane, but the maximum shear stress under plane strain is not only much lower than that under plane stress, but also on different planes, through the z axis at 45° from the x-z plane [15]. Thus, the mode and threshold stress for dislocation emission from the junction between the crack front and the free surfaces is expected to differ from the bulk. The strain ϵ_{zz} is zero and therefore the stress σ_{zz} is *not* zero in our initial setup (at $t = 0$). For $t > 0$, free surface boundary conditions are employed, which induce a dynamic transition region between surface and interior. Tensile (mode I) loading ($\sigma_{yy} > 0$) induces a Poisson-ratio contraction in the vicinity of the free surface. For the regions around the junction, the contraction is magnified around the crack tip. Figure 3(a) clearly shows that regions around the junction are indented, but those near the crack surfaces bulge out. The dynamic contraction combined with the plane stress condition punches jogging dislocations out from the junctions. The half-loop dislocations are approximately

mirror symmetric with respect to the x-z crack plane, pinning on the free surfaces near the junctions, as shown in Fig. 3(a). Similar jogging dislocation emission from the junctions has been observed experimentally in silicon [16].

We have overcome the challenging problem of visualizing these dramatic 3D phenomena inside our large computational cells by noting that the potential energies of individual atoms near free surfaces and dislocation cores are narrowly peaked at values above the cohesive (bulk) energy (about -6ε in fcc). Thus, we can select potential values within certain ranges about those peak values to render bulk atoms invisible and display the structures of dislocation loops, for example. For the Morse potential with stiffness parameter $\alpha = 7$, under free surface boundary conditions, we observe only jogging dislocation emission from the crack front. On the other hand, we find that under periodic boundary conditions, the crack tends to emit dislocations while deflecting (i.e., the crack branches) from the initial {100} plane to the {111} planes, which have a lower surface energy. Hence, we believe that this is a borderline case between ductile and brittle fracture. For $\alpha = 6$, a flat, long blunting dislocation is first emitted from the crack front, and then many jogging dislocations are ejected along it. In contrast, we observe only blunting dislocation emission along the crack front in EAM Cu [see Fig. 3(a)] (of course, at higher temperatures, dislocation lines will not be so straight). In general, the shorter the range of an interatomic potential, the harder it is to emit blunting dislocations (see [4,17]). For dislocation emission in EAM Cu, blunting is easier than jogging; thus, jogging only occurs at the junction. For Morse $\alpha = 7$, blunting dislocation emission is difficult, and therefore jogging dislocations are emitted all along the crack front. We observe that these jogging dislocation loops exhibit a bent "<" shape, where one jogging loop is above the crack front while the other is roughly mirror symmetric below, rather than a straight "\" shape, as previously conjectured [6,9,10,12]. Ledge formation energy as a function of interatomic potentials may provide a clue to understanding the switch of the dislocation emission mode.

We see primarily the same features in the process of blunting dislocation emission in the 35 million and 3.5 million atom simulations for EAM Cu (a factor of 2 in crack length and factors of 2, 2.5, and 2 in x, y, and z lengths, respectively). We therefore conclude that 3.5 million atoms is sufficiently large for realistic investigation of 3D dislocation emission, at least in the early stages. Our 35 million atom system contains 241 planes in the z direction, so that there is no intrinsic restriction on 3D dislocation emission, in contrast with previous quasi-3D simulations with a periodic thickness of two atomic layers [1,2,18]. Dislocation emission processes occur above and below the crack tip roughly in the same sequence and at the same time for both system sizes. By carefully plotting the atomic positions in a plane perpendicular to the z axis [as shown in

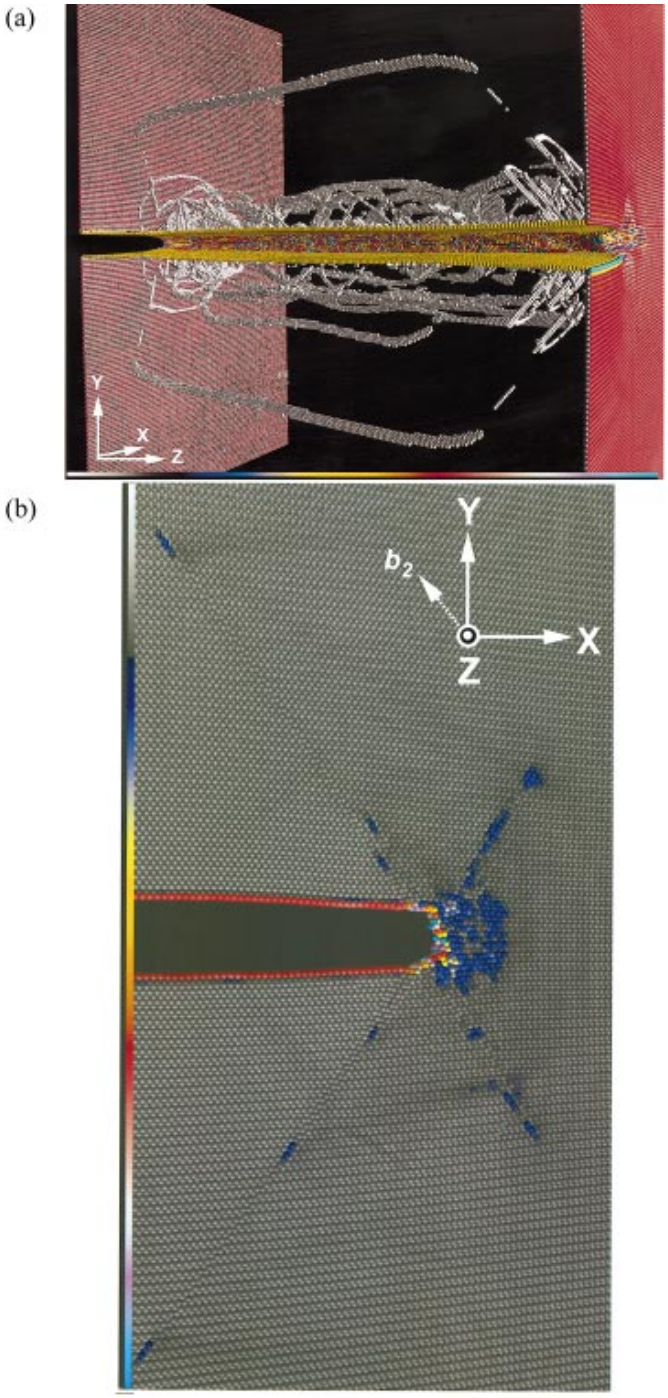

FIG. 3(color). Long straight blunting dislocation loops (shown in shadow) emitted only along the crack front and shorter jogging dislocation loops (highlighted) generated only at the junctions between free surfaces (red) and the crack front: 35 million atoms interacting via EAM Cu potential. The strain rate is $0.001 t_0^{-1}$ (about 10^9 sec^{-1}) and the time is $21 t_0$ for this image. Particles are colored by atomic potential energy; to visualize dislocation loops and the crack front, only particles with energy between -5.89ε and -3.8ε are shown (we thereby effectively reduce the 700 MB original data by a factor of $\sim$80). (a) Viewed from behind (back half of sample cut away); (b) the emission sequence shown in the $z = 0$ plane [color range slightly shifted from (a)]. Note possible Lomer dislocations $[1/2[10\bar{1}]$ on (010)], emitted from both lower and upper edges of the blunted crack.

Fig. 3(b)], we see the early-stage emission of backward-moving blunting dislocations. Beginning with the sharp tip corresponding to the elastic continuum solution, the crack advances two atomic spacings, and the tip becomes more rounded just prior to dislocation emission. Then we observe that a half-loop Shockley partial dislocation emerges at $t = 5.5t_0$ on {111} slip planes, which is very long ($\sim 190r_0$) and flat in the direction of the crack front. This indicates that a minimum length of crack front is required to accommodate the first blunting dislocation emission. Surprisingly, the first partial is ejected backward (see Figs. 2 and 3). Next, a second partial is emitted *forward* at $0.5t_0$ later. One might suppose that because the stress in the forward direction is higher than that in the backward, the first partial should be emitted in the forward direction. However, the *driving force* on the dislocation depends on the product of the stress and the Burgers vector. The pathways for forward and backward emission are shown in Fig. 2. The driving force for backward motion of the partial with b_2 is only about 3% larger than that for forward motion of the partial with b_1. With an anisotropic crack stress field, this ratio becomes about 1.30 [18]. This calculation, which is a rough continuum approximation, is consistent with the observation that the second partial dislocation is emitted forward soon after the first partial is emitted backward. By performing the Burgers circuit around the partials, we see that the Burgers vector for the backward-moving blunting dislocation is b_2, as shown schematically in Fig. 2. We have confirmed this observation by comparing with partial dislocations in an otherwise perfect crystal. Using quasi-3D MD, Hoagland [18] observed backward dislocation emission in EAM Ni, while deCelis *et al.* [2] report that two Shockley partial dislocation *lines* were emitted *forward* at $T = 300$ K for Cu. Schiøtz *et al.* [19] report that extended dislocation loops are emitted forward from a wide notch in their 3D MD simulations in Cu. (However, since the two notch surfaces are chosen to be {111} slip planes, their simulations artificially forbid backward emission.) Gumbsch and Beltz [20] also observed the backward dislocation emission in their quasi-3D molecular statics simulation in EAM Ni. It is even more striking to see that the other two partials with b_2 (the same type as the first one) are emitted backwards in *different* adjacent {111} slip planes later and leave behind a twin. With the simulations continuing up to $t = 25t_0$, we did not observe the backward emission of an extended dislocation.

With these large-scale MD simulations in 3D, we have observed for the first time unambiguous evidence of emission of blunting and jogging dislocation loops. These three-dimensional dislocation phenomena can effectively be visualized and analyzed by a new technique, where only those atoms within certain ranges of atomic potential energy are plotted. Our calculations have revealed for the first time the dynamic sequence of dislocation emission from a 3D crack tip.

Computations were performed on the TMC CM-5 and CRAY T3D at the Advanced Computing Laboratory at Los Alamos. We thank Art Voter for providing and helping implement his EAM Cu potential. We also thank Robb Thomson, Ali Argon, John Hirth, Richard Hoagland, Sid Yip, and Peter Gumbsch for helpful discussions.

[1] R. G. Hoagland, P. C. Gehlen, and J. P. Hirth, Philos. Mag. **34**, 413 (1976).
[2] B. deCelis, A. S. Argon, and S. Yip, J. Appl. Phys. **54**, 4864 (1983).
[3] P. S. Lomdahl, P. Tamayo, N. Grønbech-Jensen, and D. M. Beazley, in *Proceedings of Supercomputing 93* (IEEE Computer Society Press, Los Alamitos, CA, 1993), p. 520–527; D. M. Beazley and P. S. Lomdahl, Parallel Comput. **20**, 173 (1994).
[4] B. L. Holian and R. Ravelo, Phys. Rev. B **51**, 11 275 (1995); S. J. Zhou, P. S. Lomdahl, R. Thomson, and B. L. Holian, Phys. Rev. Lett. **76**, 2318 (1996).
[5] J. R. Rice and R. Thomson, Philos. Mag. **29**, 73 (1974).
[6] S. J. Zhou and R. Thomson, J. Mater. Res. **6**, 639 (1991).
[7] K. Y. Chia and S. J. Burns, Scr. Metall. **18**, 467 (1984).
[8] Y.-H. Chiao and D. R. Clarke, Acta Metall. **37**, 203 (1989).
[9] A. S. Argon, Acta Metall. **35**, 185 (1987).
[10] G. Schöck and W. Puschl, Philos. Mag. **64**, 931 (1991); G. Schöck, Philos. Mag. (to be published).
[11] J. R. Rice and G. E. Beltz, J. Mech. Phys. Solids **42**, 333 (1994).
[12] G. Xu, A. S. Argon, and M. Ortiz (to be published).
[13] A. F. Voter, Los Alamos Unclassified Technical Report No. LA-UR-93-3901.
[14] N. J. Wagner, B. L. Holian, and A. F. Voter, Phys. Rev. A **45**, 8457 (1992).
[15] D. Broek, *Elementary Engineering Fracture Mechanics* (Martinus Nijhoff Publishers, Boston, 1982).
[16] A. George and G. Michot, Mater. Sci. Eng. A **164**, 118 (1993).
[17] S. J. Zhou, A. E. Carlsson, and R. Thomson, Phys. Rev. Lett. **72**, 852 (1994).
[18] R. G. Hoagland, in *Proceedings of the Symposium on New Techniques for Characterizing Corrosion and Stress Corrosion* (TMS, Cleveland, 1995).
[19] J. Schiøtz, K. W. Jacobsen, and O. H. Nielsen, Philos. Mag. Lett. **72**, 245 (1995).
[20] P. Gumbsch and G. E. Beltz, Model. Simul. Mater. Sci. Eng. **3**, 597 (1995).